VOL. 14, NO. 4 J. HYDRONAUTICS OCTOBER 1980

ARTICLE NO. 79-2002R

Potential Hydroelastic Instability of Profiled Underwater Structures

L.E. Ericsson* and J.P. Reding†
Lockheed Missiles & Space Company, Inc., Sunnyvale, Calif.

Appendages on underwater vehicles are often given a cross-sectional profile that will produce low drag. The potential danger is that if the profile shape is not selected carefully, the structural integrity of the appendage may be endangered by hydroelastic instability. While static divergence is usually investigated, the potential for divergent oscillations leading to destructive amplitudes is not recognized as readily. Structural damping, which often is a saving feature for wind-induced loads, plays a completely insignificant role in a high-density fluid such as water. The unsteady hydrodynamic characteristics leading to self-excited oscillations are derived analytically and the means by which the dynamic instability can be minimized or eliminated are described.

Nomenclature

b = spanwise extent of appendage
c = local chordwise extent
c_o = root chord, $c_o = c_{\max}$
D = damping in plunging oscillations
D' = hydrodynamic drag coefficient, $c_d = (\partial D'/\partial y)/(\rho V^2/2)c$
d = maximum cross-sectional thickness
E = dissipated energy per cycle, Eq. (13)
F = hydrodynamic force, Eqs. (2,4, and 5)
k = reduced frequency parameter, $k = \bar{\omega}/2$
k_A = parameter in Eq. (20)
L = hydrodynamic lift coefficient, $c_l = (\partial L/\partial y)/(\rho V^2/2)c$
$\bar{m}$ = generalized mass, Eq. (1)
M = hydrodynamic torque coefficient, $c_m = (\partial M/\partial y)/(\rho V^2/2)c^2$
N = hydrodynamic normal force coefficient, $c_n = (\partial N/\partial y)/(\rho V^2/2)c$
$P(t)$ = generalized force, Eq. (2)
q = normalized bending coordinate
Re = Reynolds number based upon d and freestream conditions
U_∞ = vehicle speed or freestream velocity
V = local relative velocity
W = work
t = time
x_T = tail length, Fig. 15
y = spanwise coordinate, Fig. 1
z = lateral deflection, Fig. 1
α = angle of attack
α_o = local trim angle of attack
α_M = maximum local trim angle of attack, $\alpha_M = (\alpha_o)_{\max}$, Fig. 9.
Δ = increment or amplitude
ζ = damping parameter, fraction of critical damping
ζ_o = structural damping
$\zeta_a + \zeta_s$ = hydrodynamic damping
θ = angle-of-attack perturbation
η = dimensionless y coordinate, $\eta = y/b$
ξ_o, a = location of elastic axis in fraction of local chord, $\xi_o = (1+a)/2$
$\Delta\xi_t$ = parameter in Eq. (20)
ρ = fluid density
υ = trailing-edge angle, Fig. 13
ϕ = normalized bending mode
ψ = phase angle, $\psi = \omega t$
$\omega, \bar{\omega}$ = natural frequency, $\bar{\omega} = \omega c/V$

Subscripts

a = attached flow
f = buffeting force
lim = limit
M = tip value
s = separated flow
TH = theoretical value for attached flow
0 = initial value
$1,2,3$ = numbering subscripts in Eq. (16)
∞ = undisturbed flow

Superscript

i = induced (e.g., $\Delta^i c_{n\theta}$ separation-induced sectional normal force derivative)

Derivatives

$c_{m\dot{z}} = \partial c_m/\partial(\dot{z}/V)$
$c_{n\theta} = \partial c_n/\partial\theta$
$c_{\bar{n}\dot{z}}$ = effective damping derivative defined by Eq. (15)
$\ddot{q} = \partial^2 q/\partial t^2$
$\dot{\theta} = \partial\theta/\partial t$

Presented as Paper 79-2002 at AIAA/SNAME 5th Conference on Advanced Marine Vehicles, Baltimore, Md., Oct. 2-4, 1979; submitted Oct. 29, 1979; revision received April 17, 1980.

Index categories: Hydrodynamics; Nonsteady Aerodynamics; Jets, Wakes, and Viscid-Inviscid Flow Interactions.

*Senior Consulting Engineer. Associate Fellow AIAA.
†Staff Engineer. Associate Fellow AIAA.

Introduction

THE underwater appendage considered is a long, cantilevered structure typical of telemetry receiving antennae used to collect flight performance data from submarine-launched missiles. Such temporary masts are neither retractable nor are they designed to the same rigorous specifications as the rest of the submarine. They must, therefore, be designed to cope with the hydrodynamic forces induced by sea currents and the motion of the submarine.

When the conventional circular cross section cannot be used because of drag considerations, a profiled shape is a natural choice. The present paper discusses how the partial flow separation occurring on such nonslender cross sections leads to dynamic stability problems similar to those of "galloping cables." Although the cross section determines the dynamic

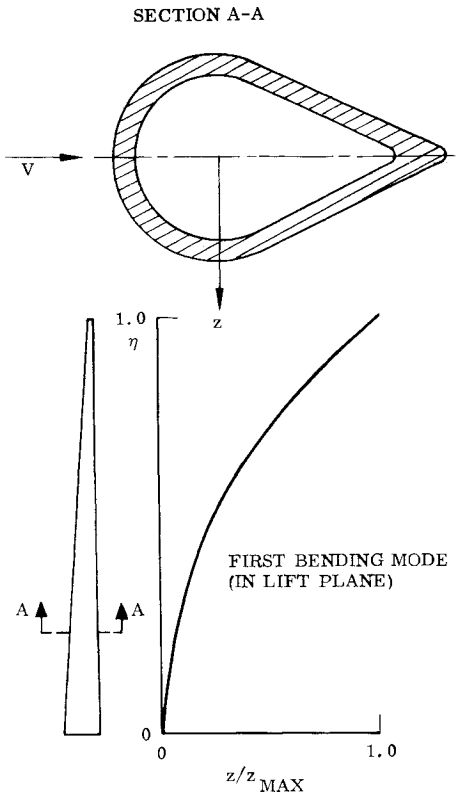

Fig. 1 Geometry and deflection mode shape of underwater appendage.

instability, which therefore is not restricted per se to long, cantilevered structures, the hydroelastic problem analyzed here is for such a configuration.

Discussion

The structural integrity of the mast will depend almost entirely upon the hydroelastic characteristics. Because the structural damping is usually negligible for typical underwater velocities, positive hydrodynamic damping is required to limit elastic oscillations to amplitudes of acceptable magnitude.

An example of a low-drag underwater appendage of nearly optimized structural design is shown in Fig. 1. Figure 2 shows the experimental lift characteristics for a closely similar teardrop-shaped cross section.[2] It will be demonstrated that the negative lift slope for $\alpha<20$ deg can produce bending oscillations (mode shape shown in Fig. 1) of unacceptable magnitude. Various changes that can be made to the profile shape in order to eliminate the negative lift slope will be discussed. Of the possible fixes, the one usually preferred by the design engineer will be discussed at length

Hydroelastic Analysis

The underwater structure illustrated in Fig. 1 will be analyzed for bending oscillations. The equations of motion can be written in the following form using standard notations

$$\tilde{m}[\ddot{q}(t)+2\zeta_o\omega\dot{q}(t)+\omega^2 q(t)]=P(t) \tag{1}$$

The generalized force $P(t)$ is given by the virtual work done by the hydrodynamic forces and moments. (If W is the work done, $P=\partial W/\partial q$.)

For the bending degrees of freedom $P(t)$ is

$$P(t)=\int \frac{\mathrm{d}F}{\mathrm{d}y}\phi(y)\mathrm{d}y \tag{2}$$

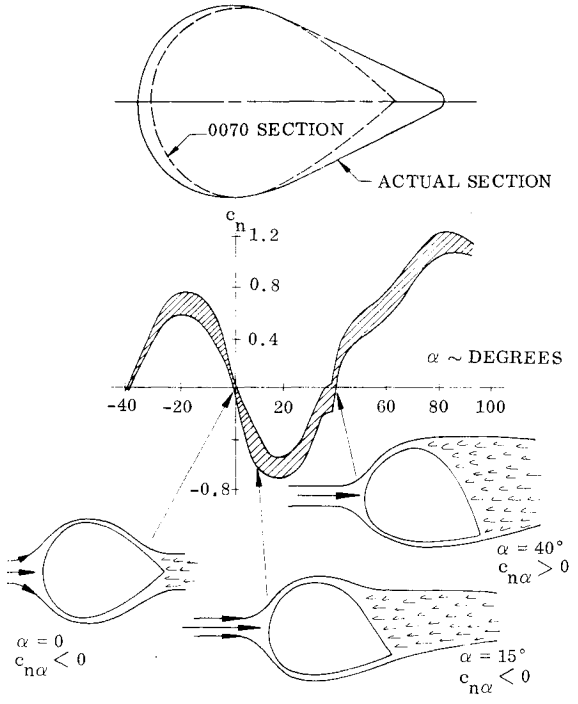

Fig. 2 Normal force characteristics of 0070 section.

where

$\frac{dF}{\mathrm{d}y}$ = normal force per unit span

$\phi(y)$ = normalized bending mode

There are three different types of generalized force

$$P(t) = P_s(t)+P_a(t)+P_f(t) \tag{3}$$

where

$P_s(t)$ = generalized force in separated flow

$P_a(t)$ = generalized force in attached flow

$P_f(t)$ = generalized force independent of body motion (e.g., due to buffeting or vortex wakes).

In Fig. 1 the local cross-flow velocity is V. For small perturbations z the section hydrodynamic force induced by separated flow can be expressed in derivative form as follows (the hydrodynamic acceleration derivatives are assumed negligible compared to the structural counterparts)

$$\frac{\mathrm{d}F_s}{\mathrm{d}y}=\frac{\rho V^2}{2}c\Delta^i c_{n\theta}\frac{\dot{z}}{V} \tag{4}$$

The corresponding expression for the attached-flow derivatives is

$$\frac{\mathrm{d}F_a}{\mathrm{d}y}=\frac{\rho V^2}{2}cc_{n\theta}\frac{\dot{z}}{V} \tag{5}$$

For pure bending oscillations Eqs. (1-5) give the following results‡

$$\ddot{q}(t)+2\omega(\zeta_o+\zeta_a+\zeta_s)\dot{q}(t)+\omega^2 q(t)=\frac{P_f(t)}{\tilde{m}} \tag{6}$$

‡All hydrodynamic interference-type terms, $c_n(z)$, associated with the depth z of the cross section below the water surface, have been assumed negligible.

ζ_a and ζ_s are defined as follows[3]:

$$\zeta_a+\zeta_s=\int_o^b \frac{\rho Vc}{4\omega\bar{m}}\left(c_{n\theta}+\Delta^i c_{n\theta}\right)\phi^2(y)\,dy \tag{7}$$

where $y=\eta b$.

Hydrodynamic Damping

It can be seen from Eq. (6) that a necessary condition for bounded oscillations is the following

$$\zeta_o+\zeta_a+\zeta_s>0 \tag{8}$$

Equation (7) shows that in absence of forcing functions, $P_f(t)=0$, aeroelastic instability will only occur if the total normal force slope, $c_{n\theta}+\Delta^i c_{n\theta}$, is negative.

Figure 2 shows that the gradually increasing separation on the leeward side causes a negative lift curve slope up to $\alpha=20$ deg. At higher angles of attack the leeside of the section no longer dominates, because the separation point moves little with further α increase. Consequently, a positive lift slope is realized for $\alpha>20$ deg. The results in Fig. 2 will be approximated as follows for the unsteady hydrodynamic analysis

$$c_{n\alpha}=\begin{cases}-3.0: & |\alpha|<20\,\text{deg}\\ 2.0: & 20\,\text{deg}\le\alpha\le 90\,\text{deg}\end{cases} \tag{9}$$

Using Fig. 1 the lateral deflection z at $y=\eta b$ is given as follows for harmonic oscillations

$$z=\Delta z\sin\omega t$$

$$\Delta z=\Delta z_o\phi(\eta) \tag{10}$$

The lateral rate of deflection induces the following effective angle of attack

$$\tilde{\alpha}=\alpha_o+\frac{\dot{z}}{V}=\frac{\Delta z}{c}\bar{\omega}\cos\omega t$$

$$\bar{\omega}=\omega c/V \tag{11}$$

Nonlinear Damping Analysis

The nonlinear damping analysis of Ref. 4, which in turn is an extension of the methods presented in Ref. 5, will be modified to apply to the present case of plunging or bending oscillations. In the linear case the damping derivative $c_{n\dot{z}}$ is simply

$$c_{n\dot{z}}=c_{n\theta}+\Delta^i c_{n\theta}=(c_{n\alpha})_s \tag{12}$$

In the nonlinear case one can define a linear measure $c_{\bar{n}\dot{z}}$ of the energy dissipation per oscillation cycle, which becomes $c_{n\dot{z}}$ when the nonlinearity disappears. For oscillations $z=\Delta z\sin\omega t$ one obtains the following expressions for the energy dissipation per cycle

$$E=-\int c_n\,dz=-c_{\bar{n}\dot{z}}\int\frac{\dot{z}}{V}\,dz \tag{13}$$

That is

$$c_{\bar{n}\dot{z}}=\int_{t_o}^{t_o+2\pi/\omega} c_n\dot{z}\,dt\Big/\int_{t_o}^{t_o+2\pi/\bar{\omega}}\left(\frac{\dot{z}}{V}\right)\dot{z}\,dt$$

$$=\int_{\psi_o}^{\psi_o+2\pi} c_n\cos\psi\,d\psi\Big/\pi\bar{\omega}\Delta\zeta \tag{14}$$

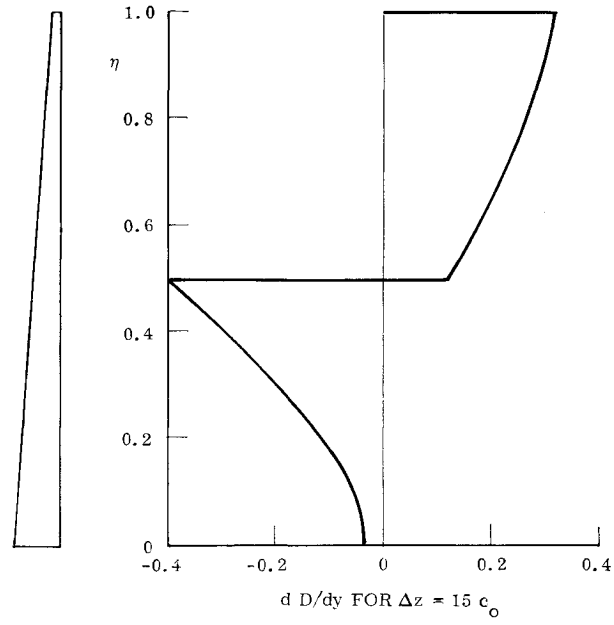

Fig. 3 Damping distribution for first bending mode at $\alpha_o=0$ and $U_\infty=16$ knots.

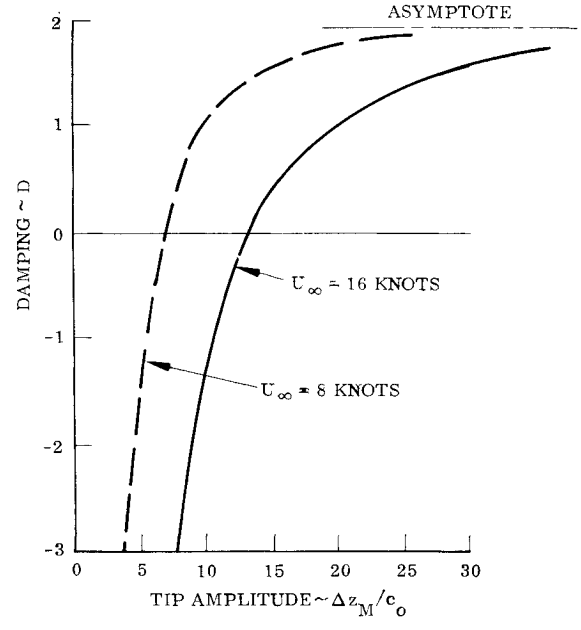

Fig. 4 Net damping for first bending mode at $\alpha_o=0$.

or

$$c_{\bar{n}\dot{z}}=\frac{2}{\pi\bar{\omega}\Delta\xi}\int_{\psi_o}^{\psi_o+\pi} c_n\cos\psi\,d\psi \tag{15}$$

Rather than using a high-degree odd power polynomial to describe c_n from data of the type shown in Fig. 2 one can use a set of linear branches, which often will fit the data better than a polynomial.

$$c_n=\begin{cases}c_{n\alpha_1}\dfrac{\dot{z}}{V} & :\left|\dfrac{\dot{z}}{V}\right|<\alpha_1\\ c_{n\alpha_1}\alpha_1+c_{n\alpha_2}\left(\dfrac{\dot{z}}{V}-\alpha_1\right) & :\alpha\le\left|\dfrac{\dot{z}}{V}\right|<\alpha_2\\ c_{n\alpha_1}\alpha_1+c_{n\alpha_2}(\alpha_2-\alpha_1)+c_{n\alpha_3}\left(\dfrac{\dot{z}}{V}-\alpha_2\right) & :\left|\dfrac{\dot{z}}{V}\right|\ge\alpha_2\end{cases} \tag{16}$$

Combining Eqs. (15) and (16) gives

$$c_{n\dot{z}} = c_{n\alpha_1} + \frac{2}{\pi}\left(c_{n\alpha_2} - c_{n\alpha_1}\right)\left[\arccos\left(\frac{\alpha_1}{\Delta\zeta\bar{\omega}}\right) - \frac{\alpha_1}{\Delta\zeta\bar{\omega}}\sqrt{1-\left(\frac{\alpha_1}{\Delta\zeta\bar{\omega}}\right)^2}\right] + \frac{2}{\pi}\left(c_{n\alpha_3} - c_{n\alpha_2}\right)\left[\arccos\left(\frac{\alpha_2}{\Delta\zeta\bar{\omega}}\right) - \frac{\alpha_2}{\Delta\zeta\bar{\omega}}\sqrt{1-\left(\frac{\alpha_2}{\Delta\zeta\bar{\omega}}\right)^2}\right] \tag{17}$$

For large amplitudes, when $(\alpha_1/\Delta\zeta\bar{\omega})^2 < (\alpha_2/\Delta\zeta\bar{\omega})^2 \ll 1$, Eq. (17) simplifies to

$$c_{\hat{n}\dot{z}} = c_{n\alpha_3} - \frac{2}{\pi\Delta\zeta\bar{\omega}}\left[(c_{n\alpha_2} - c_{n\alpha_1})\alpha_1 + (c_{n\alpha_3} + c_{n\alpha_2})\alpha_2\right] \tag{18}$$

For the approximation of the data in Fig. 2, expressed in Eq. (9), one obtains

$$c_{n\alpha_1} = -3.0,\ c_{n\alpha_2} = 2.0,\ c_{n\alpha_3} = 0$$

$$\alpha_1 = 20\ \text{deg} = 0.35 \text{ and } \alpha_2 = 90\ \text{deg} = 1.57$$

Using this in Eq. (17) or (18) gives the effective local damping derivative. For uniform flow, $V = U_\infty = 16$ knots and the tip amplitude $\Delta z_M/c_o = 15$, the spanwise damping distribution shown in Fig. 3 is obtained. The figure shows how the negative damping of the inner sections, where the effective angle of attack is less than 20 deg, is balanced by the positive damping of the outer sections. The integrated net damping as a function of amplitude is shown in Fig. 4 for $U_\infty = 8$ and 16 knots. The figure gives the limit cycles $(\Delta z_M/c_o)_{\text{lim}} = 6.5$ and 13 for the two velocities. As the structural damping has a negligible effect, oscillations will diverge (or converge) to the amplitude giving zero net hydrodynamic damping. Even for $U_\infty = 8$ knots the limit cycle amplitude is $\Delta z_M/c_o = 6.5$, meaning that the tip amplitude is 6.5 root chords. For the particular design considered this was 20% beyond the structural capability. Thus, the design had to be changed.

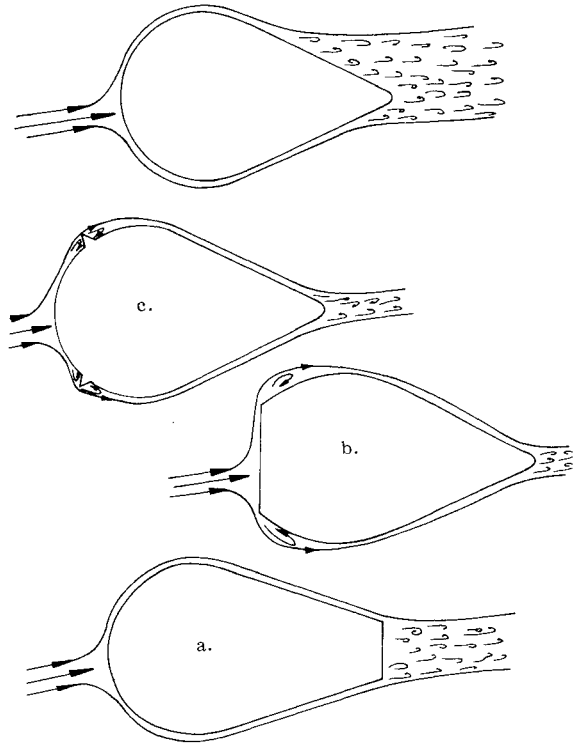

Fig. 5 Modifications causing attached flow at $\alpha \leq 10$ deg.

Possible Fixes

The only realistic way to improve the situation is to change the hydrodynamic characteristics of the cross section. Structural means are inefficient. If the stiffness were doubled, doubling $\bar{\omega}$ in Eq. (14), the effect would be the same as decreasing U_∞ from 16 to 8 knots, provided that $\phi(\eta)$ remains the same. The root of the problem is the leeside separated flow region (Fig. 2).[3] Changing the boattail angle (e.g., by increasing the trailing-edge thickness, Fig. 5a) would delay separation to an angle of attack $\alpha_s > 0$. Other means of obtaining this result through so called "preseparation effects"[4] are shown in Figs. 5b and 5c. "Fixes" illustrated in Figs. 5b and 5c would cause a drag increase, whereas the shape shown in Fig. 5a is likely to cause a drag decrease.

If the above fixes are successful, the cross-sectional characteristics will approach those of a regular airfoil, such as NACA 0012 (Fig. 6), although the lift slope $c_{l\alpha}$ may not be as high. In this case one has to be concerned with the effect of sudden, total separation of the leeside flow at a certain angle of attack, $\alpha = \alpha_s$. This is the dynamic stall problem, which already has been investigated extensively (see Ref. 6 for a recent review of the state-of-the-art). When normalizing the damping relative to the attached flow or theoretical value, the results of an analysis for an airfoil, such as the NACA 0012 (Fig. 6), become applicable to the present cross section.

An analytical technique has been developed that can, after the latest extensions, fully describe the unsteady aerodynamic characteristics of an airfoil describing torsional oscillations in the stall region.[7,8] But for an airfoil describing translatory or plunging oscillations in the stall region, further development is needed before quantitative prediction is possible. Qualitative prediction was, however, demonstrated in Ref. 6, and the present analytic capability provides the tool necessary for "analytic extrapolation" from experimental data in the present analysis. Liva et al.[9] have measured the "damping in plunge" of airfoils describing translatory oscillations at trim angles of attack near stall, $\alpha_o \approx \alpha_s$ (Fig. 7). As can be seen, the oscillations may be undamped for $\alpha_o \geq \alpha_s$. Whether or not negative aerodynamic damping is encountered depends upon the magnitude of $\tilde{\alpha}$, see Eq. (4). Thus, $|\tilde{\alpha}| = \bar{\omega}\Delta z/c_o = \omega\Delta z/U_\infty$ is the relevant parameter. The decrease of damping due to stall is inversely proportional to this parameter.[6] Figure 8 shows that the experimental results of Ref. 9 are bounded by

$$\frac{\Delta_s D}{D_{TH}} = -0.08\Big/\frac{\omega\Delta z}{U_\infty} \tag{19}$$

Using this upper limit gives the results shown in Fig. 9. The figure shows how the stalling outer sections decrease the damping from the attached flow or theoretical level. The top part of the figure, representing a continuously changing cross section, shows results that are idealized to the extent that it is assumed that stall starts at a spanwise location (η) when $\alpha(\eta) = \alpha_s$. Helicopter stall flutter tests[10] indicate that the spanwise correlation effect of the blade oscillations in bending causes the flow separation to spread inboard. Thus, the stall did not start at the tip and spread gradually inboard with increasing α; instead, stall started simultaneously on the outer 40% of the blade. But from the observed effect of flow fences and chord discontinuities on wing stall, one would expect that for a geometry representing a telescoping structure, such as that shown in the bottom part of Fig. 9, the stall would jump from section to section. Consequently, the damping

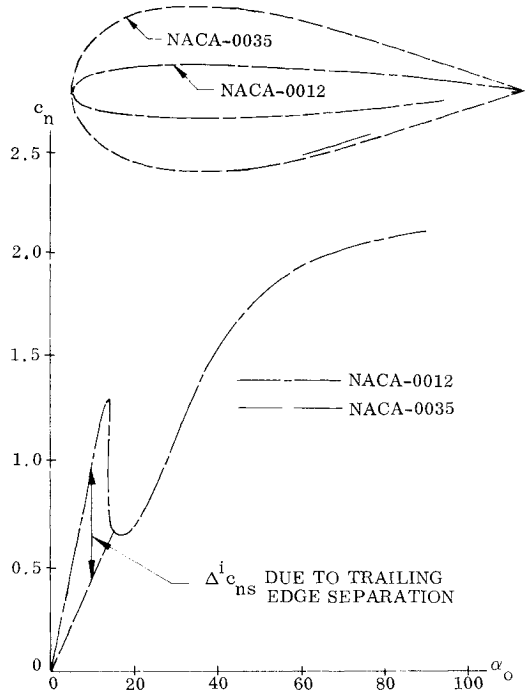

Fig. 6 Typical airfoil characteristics.

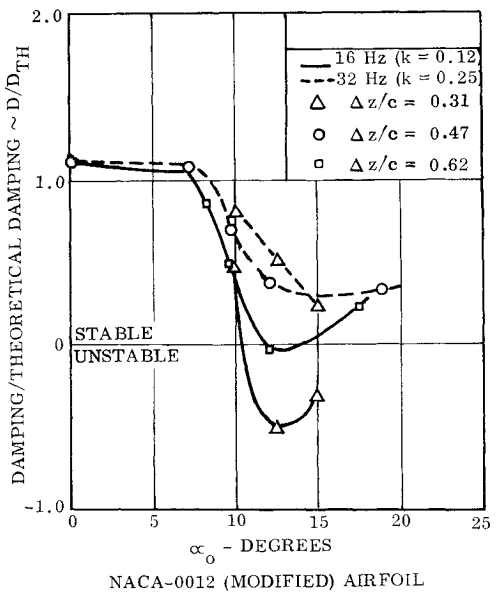

Fig. 7 Measured damping in plunge at high angles of attack (Ref. 9).

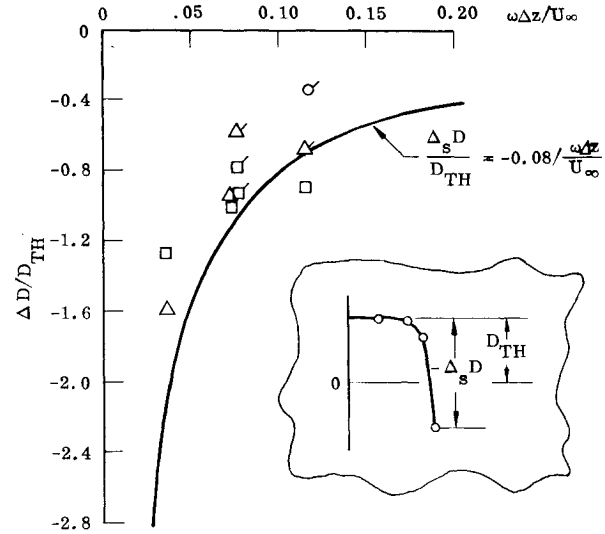

Fig. 8 Effect of stall on "damping in plunge" for airfoils such as NACA 0012.

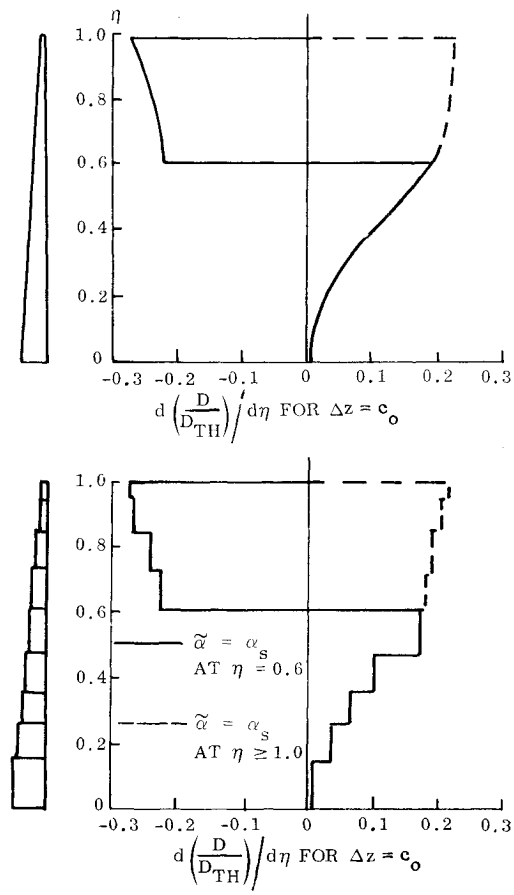

Fig. 9 Damping distributions for first bending mode of appendage with NACA 0012 cross sections.

distribution for the telescoping design is more realistic, and its integrated net damping is used, giving the results shown in Fig. 10 for different angles of attack at $U_\infty = 16$ knots. The limit cycle amplitude, the Δz value giving $D/D_{TH} = 0$, is of rather modest magnitude compared with the results of Fig. 4.

Whereas the limit cycle amplitude for the original cross-section in Fig. 4 is largest for $\alpha_o = 0$, the limit cycle amplitude for the modified cross-section in Fig. 10 is maximum for a certain trim angle $\alpha_o > 0$. The local trim angle along the span will vary because of waves and vehicle motion. Figure 11 shows this distribution for a critical design condition and the resulting limit cycle amplitude at $U_\infty = 16$ knots as a function of the trim angle of attack α_M at the tip. It can be seen that $(\Delta z/c_o)_{\lim} \leq 1.5$ (i.e., it is one order of magnitude less than what was obtained earlier using the 0070 section aerodynamic characteristics). It is true that the stresses due to this amplitude have to be added to the static and random loads. Even so, the results are very promising. It should be possible to assure hydroelastic stability by changing the cross section along the lines illustrated in Fig. 5. But in order to assure such results, a limited amount of testing is needed. It may suffice to obtain flow visualization, which could easily be accomplished by using a hydrodynamic facility, in which case three-component measurements could also be made. A quick solution to the problem may be to use a cylindrical section, provided that the drag is acceptable. A good compromise would be to use an airfoil-like profile for the inner sections and a circular cross-section for the outer sections.

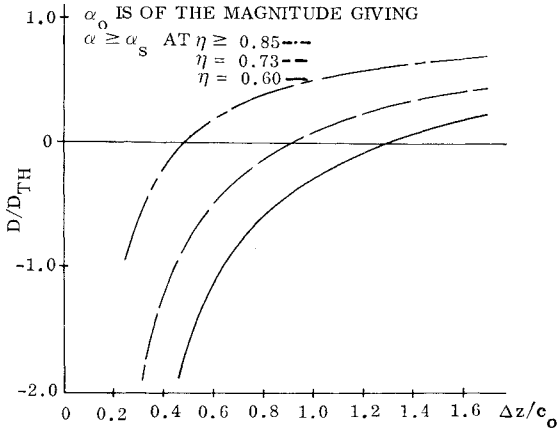

Fig. 10 Net damping of first bending mode at various α_o for appendage with NACA 0012 cross section.

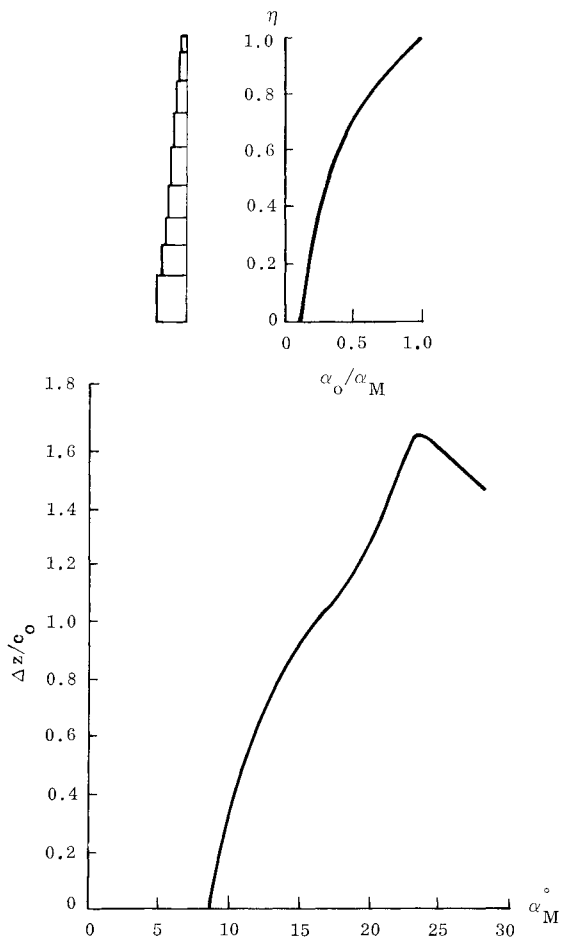

Fig. 11 Effect of maximum angle of attack α_M on damping of appendage with NACA 0012 cross section.

Design Solution

A design solution that eliminates the problem is as follows. The profile on the inner sections is changed so that attached flow is maintained up to the angles of attack of interest, and a circular cross-section is used for the outer sections where the attached flow lift would cause too large, static, lateral loads.

Static Characteristics

The extent of the trailing edge stall at $\alpha = 0$ can be inferred from the sectional drag curve[11] (Fig. 12). The negative lift occurs as the leeside separation moves upstream and the windward separation downstream for $\alpha > 0$, as is shown in Fig. 2 for a similar section.[3]

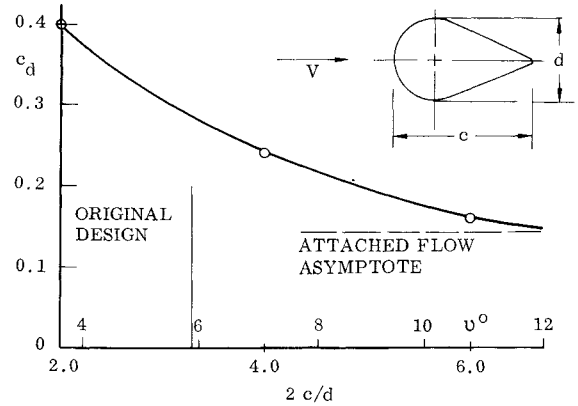

Fig. 12 Drag of faired cylinders (Ref. 11).

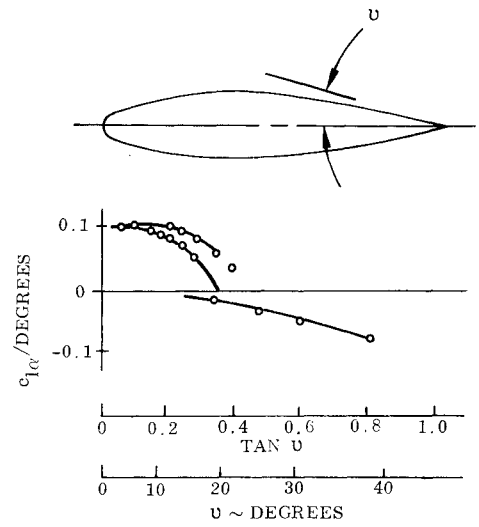

Fig. 13 Effect of trailing-edge angle on lift curve slope (Ref. 11).

To positively assure hydroelastic stability, it is necessary to avoid trailing-edge stall. This can be accomplished in three ways: 1) eliminating lift effects by using cylindrical mast sections, 2) eliminating stall via preseparation, or 3) designing a section that has attached flow throughout the α range of interest. Preseparation, whether induced by a blunt leading edge or by spoilers (Fig. 5), adds complication by providing a source of fluctuating pressure, adding another random forcing function. Furthermore, experimental verification and possibly some cut-and-try testing may be necessary to assure that preseparation eliminates stall. Consequently, it is best that the mast sections be either cylindrical or designed to maintain attached flow.

The slope of the airfoil trailing edge determines whether or not trailing-edge stall occurs. Hoerner's correlation[2] (Fig. 13) shows that for trailing-edge angles greater than 11.3 deg ($\nu = \tan^{-1} 0.2$) the lift curve slope ($c_{l\alpha}$) begins to decrease due to trailing-edge stall effects, until at $\upsilon = 20$ deg a negative lift slope results.

It was shown earlier that dynamic stall would not pose a problem if the hydrodynamic characteristics of the cross section were similar to those for the NACA 0012 foil shape. Thick airfoil data[12-14] indicate that the analysis performed using the thinner NACA 0012 foil shape is conservative. Thus, the extent to which the attached-flow-type inner foil section can be used will not be determined by dynamic stall reasons, but rather by static lift considerations for the angles of attack corresponding to the critical sea state (see Fig. 14). Thus, outside of a certain spanwise station, a nonlifting cylindrical section should be used.

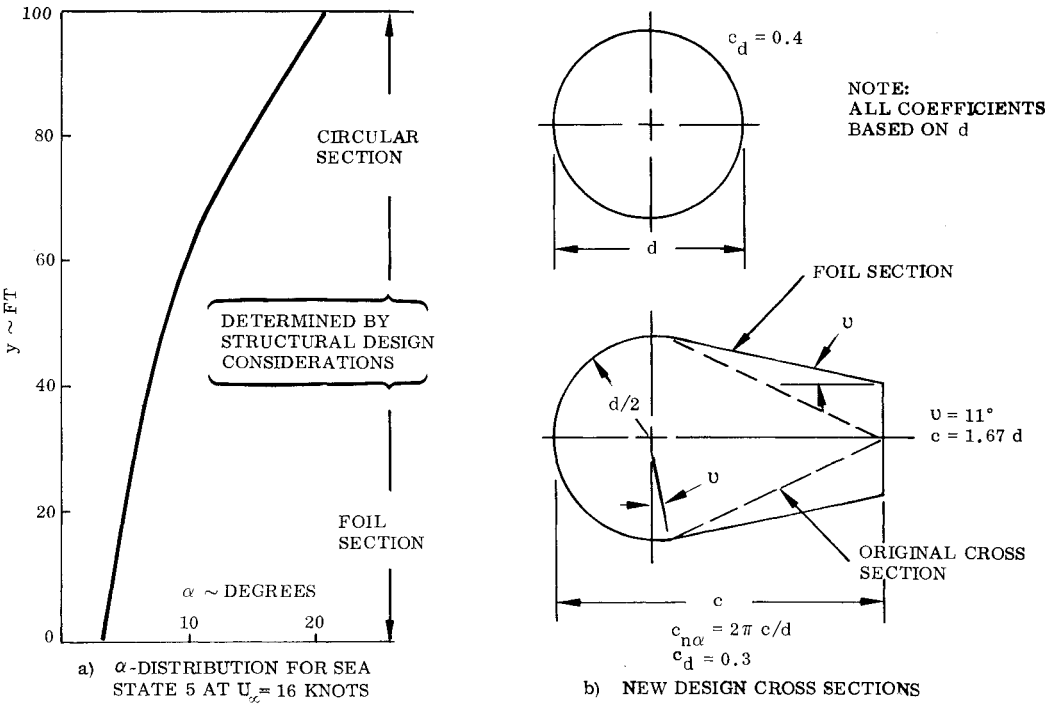

Fig. 14 Recommended cross sections.

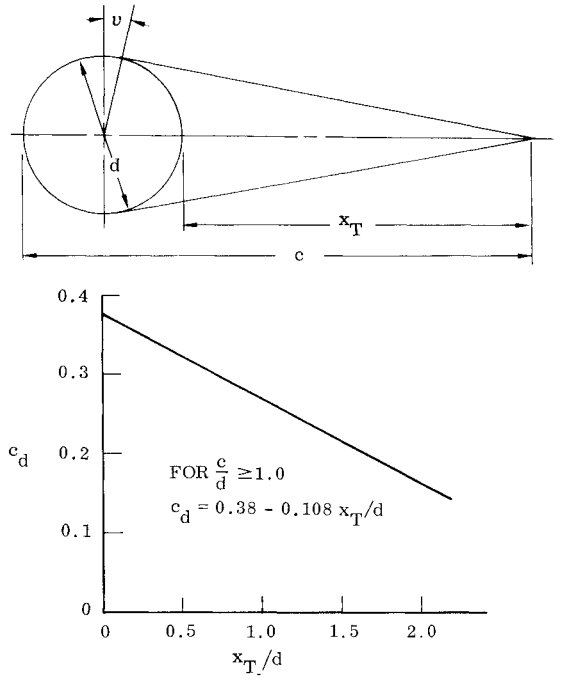

Fig. 15 Effect of fairing length on drag coefficient at $\alpha = 0$ (Ref. 2).

The proposed cross-sectional (foil) shape (Fig. 14) is a modification of the original section: the trailing-edge angle (ν) is reduced to avoid trailing-edge stall. Tests in a water tunnel have confirmed that the selected boattail angle $\nu = 11$ deg assures attached-flow behavior up to the stall angle. The blunt trailing edge is the result of constraining the airfoil section to the same cross-sectional envelope as the original section. The sectional drag force is extremely sensitive to the boattail length (Fig. 15), whereas data indicate that clipping the trailing edge does not significantly alter $c_{l\alpha}$ based upon the actual chord length c (see Fig. 16).[2]

Unsteady Characteristics

With attached flow assured on the inner mast sections by the means previously discussed, one can obtain a satisfactory estimate of the unsteady hydrodynamic characteristics using thin airfoil theory. The following "motion-dependent" normal (lateral) force and pitching (torsional) moment per unit span are obtained[6,15] (the wake induced forcing function has to be added):

$$\partial D(t)/\partial y = \rho_\infty U_\infty^2 d\left[0.19 - 0.054\left(\frac{c}{d} - 1\right)\right] \tag{20a}$$

$$\partial N(t)/\partial y = \pi\rho_\infty U_\infty^2 c\left\{k_A(\alpha_o + \theta) - \left(k_A\Delta\xi_t - \frac{1}{4}\right)\frac{c\dot\theta}{U_\infty} - \frac{1}{4}\left(\xi_o - \frac{1}{2}\right)\frac{c^2\ddot\theta}{U_\infty^2} + k_A\frac{\dot z}{U_\infty} - \left(k_A\Delta\xi_t - \frac{1}{4}\right)\frac{c\ddot z}{U_\infty^2}\right\} \tag{20b}$$

$$\partial M(t)/\partial y = \pi\rho_\infty U_\infty^2 c^2\left\{k_A\left(\xi_o - \frac{1}{4}\right)(\alpha_o + \theta) - \left[k_A\Delta\xi_t\left(\xi_o - \frac{1}{4}\right) - \frac{1}{4}\left(\xi_o - \frac{1}{2}\right)\right]\frac{c\dot\theta}{U_\infty} - \frac{1}{4} \times \left[\left(\xi_o - \frac{1}{2}\right)^2 + \frac{1}{32}\right]\frac{c^2\ddot\theta}{U_\infty^2} + k_A\left(\xi_o - \frac{1}{4}\right)\frac{\dot z}{U_\infty} - \left[k_A\Delta\xi_t\left(\xi_o - \frac{1}{4}\right) - \frac{1}{4}\left(\xi_o - \frac{1}{2}\right)\right]\frac{c\ddot z}{U_\infty^2}\right\} \tag{20c}$$

$$\Delta\xi_t = \begin{cases} 1.5 & : \ \bar\omega < 0.16 \\ \dfrac{0.245}{\bar\omega} & : \ \bar\omega \geq 0.16 \end{cases} \tag{20d}$$

$$k_A = \begin{cases} 1 & : \ \omega < 0.16 \\ 0.475\left(1 + \dfrac{1}{\sqrt{10\bar\omega}}\right) & : \ \omega \geq 0.16 \end{cases} \tag{20e}$$

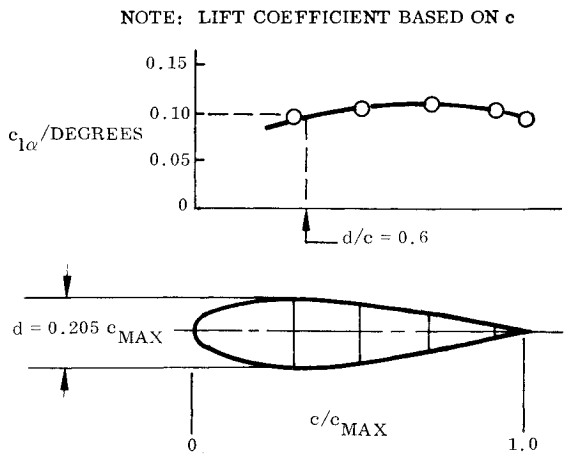

Fig. 16 Effect of trailing-edge bluntness (Ref. 11).

The above can be translated into the vernacular of the structural dynamicist with the following identities

$$\bar{\omega}=\frac{\omega c}{U_\infty}=2k \quad : \quad \xi_0=(1+a)/2 \tag{21}$$

For the cylindrical outer sections the motion-dependent hydrodynamic force and moment are as follows, based upon Hoerner's supercritical drag value,[11] i.e., $c_d=0.4$ for $Re>0.5\times10^6$.

$$\partial D(t)/\partial y=\rho_\infty U_\infty^2 d[0.200\pm0.014] \tag{22a}$$

$$\partial N(t)/\partial y=\rho_\infty U_\infty^2 d\left\{0.2\left(\alpha_o+\theta+\frac{\dot{z}}{U_\infty}\right)+\frac{\pi}{4}\frac{d\ddot{z}}{U_\infty^2}\right\} \tag{22b}$$

$$\partial M(t)/\partial y=\rho_\infty U_\infty^2 d^2\left\{0.2\left(\xi_o-\frac{1}{2}\right)\left(\alpha_o+\theta+\frac{\dot{z}}{U_\infty}\right)+\frac{\pi}{4}\left(\xi_o-\frac{1}{2}\right)\frac{d\ddot{z}}{U_\infty^2}\right\}^{\S} \tag{22c}$$

A classical binary flutter analysis using the hydrodynamic characteristics in Eqs. (20) and (22) and the structural characteristics for the telescoping design gave a flutter velocity that was several orders of magnitude larger than the design velocity, $U_\infty=16$ knots.

For the final evaluation one needs to add the wake-induced forcing function, $P_f(t)$ in Eq. (3), to the hydrodynamic characteristics of Eqs. (20) and (22). A review of the wake-induced forcing function for both cylinders and airfoils is given in Ref. 16. Note that assuming unit correlation over complete spanwise sections would be grossly overconservative, as the experimental results[16] indicate correlation lengths of, at most, 4.5 calibers can again be expected at $Re>3.5\times10^6$. Even more important is the lock-in phenomenon discussed in Ref. 17, which shows that strong coupling between the body motion and the cylinder vortex shedding can occur even when the structural frequency is far from the Strouhal frequency for the von Kármán vortex shedding. It is also shown that a blunt trailing edge should not have any shoulder roundness, because it greatly increases the vibration induced by the (von Kármán-type) vortex wake leaving the trailing edge. Even when correlated over complete spanwise sections the wake-induced forces were modest and caused no concern for the actual mast design considered.

§For the usual elastic axis location, $\xi_o=\frac{1}{2}$, the moment is zero.

Conclusions

A hydroelastic stability analysis of appendages on underwater vehicles has shown that teardrop cross sections, chosen to minimize drag, can cause limit cycle oscillations of such magnitude as to result in structural failure. The cause of the problem is flow separation, which causes the cross-sectional lift to be negative over a significant angle-of-attack range. Because the structural damping is of negligible magnitude relative to the hydrodynamic undamping, the only solution is to eliminate the flow separation generating the negative lift. This can be done by reducing the boattail angle or using preseparation devices. If drag is of no concern and the wake-induced vibrations are of tolerable magnitude, a circular cross section can eliminate lift completely, which is sometimes needed to limit the static loads. A practical design using a combination of these solutions is demonstrated.

References

[1] Parkinson, G.V., "Aeroelastic Galloping in One Degree of Freedom," *Proceedings of the Conference on Wind Effects on Buildings and Structures*, National Physics Laboratory, England, June 1963; Vol. 2, HMSO, London, 1965, pp. 582-609.

[2] Hoerner, S.F., *Fluid-Dynamic Lift-Practical Information on Aerodynamic and Hydrodynamic Lift*, Hoerner Fluid Dynamics, Brick Town, N.J., pp. 2-6—2-11.

[3] Ericsson, L.E. and Reding, J.P., "Analysis of Flow Separation Effects on the Dynamics of a Large Space Booster," *Journal of Spacecraft and Rockets*, Vol. 2, July-Aug. 1965, pp. 481-490.

[4] Ericsson, L.E., "Aeroelastic Instability Caused by Slender Payloads," *Journal of Spacecraft and Rockets*, Vol. 4, Jan. 1967, pp. 65-73.

[5] Ericsson, L.E., "Separated Flow Effects on the Static and Dynamic Stability of Blunt Nosed Cylinder-Flare Bodies," NASA CR 76919, Dec. 1965.

[6] Ericsson, L.E. and Reding, J.P., "Dynamic Stall Analysis in Light of Recent Numerical and Experimental Results," *Journal of Aircraft*, Vol. 13, April 1976, pp. 248-255.

[7] Ericsson, L.E. and Reding, J.P., "Quasi-Steady and Transient Dynamic Stall Characteristics," Paper 24 presented at AGARD Symposium on Prediction of Aerodynamic Loading, Moffett Field, Calif., Sept. 27-29, 1976, AGARD CP-204.

[8] Ericsson, L.E., and Reding, J.P., "Dynamic Stall at High Frequency and Large Amplitude," *Journal of Aircraft*, Vol. 16, Dec. 1979, pp. 136-142.

[9] Liiva, J., Davenport, F.J., Gray, L., and Walton, I.C., "Two-Dimensional Tests of Airfoils Oscillating Near Stall," USAAVLABS TR 68-13, April 1968.

[10] Tarzanin, F.J., Jr., "Prediction of Control Loads Due to Blade Stall," *Journal of American Helicopter Society*, Vol. 17, April 1972, pp. 33-46.

[11] Hoerner, S.F., *Fluid-Dynamic Drag*, Hoerner Fluid Dynamics, Brick Town, N.J., 1958.

[12] Abbott, I.H., and Van Doenhoff, A.E., *Theory of Wing Sections*, Dover Publications, Inc., New York, 1958.

[13] Stack, J., "Tests of Airfoil Designed to Delay the Compressibility Burble," NACA Report 763, 1939.

[14] Bullivanti, W.K., "Tests of the NACA 0025 and 0035 Airfoils in the Full-Scale Wind Tunnel," NACA Report 708, 1939.

[15] Ericsson, L.E. and Reding, J.P., "Unsteady Airfoil Stall, Review and Extension," *Journal of Aircraft*, Vol. 8, Aug. 1971, pp. 609-616.

[16] Schlinker, R.H., Fink, M.R., and Amiet, R.K., "Vortex Noise from Non-Rotating Cylinders and Airfoils," AIAA Paper 76-81, Washington, D.C., Jan. 1976.

[17] Ericsson, L.E., "Karman Vortex Shedding and the Effect of Body Motion," *AIAA Journal*, Vol. 18, Aug. 1980, pp. 935-944.